Chapter 2

A potential mechanism for the initial formation of sequences of barrier islands

Abstract

An idealized model is developed and analyzed to demonstrate the potential relevance of tidal motion for the emergence of undulations of a sandy coastline. These undulations might trigger the formation of inlets and barrier islands. The model describes the feedback between depth-averaged tidal and steady flow on the inner shelf, sediment transport in the nearshore zone and an irregular coastline. It is demonstrated that an initially straight coastline can become unstable with respect to perturbations with a rhythmic structure in the alongshore direction. Using parameter values that are representative for the Dutch coast, it is found that perturbations with a length scale smaller than 8 km will grow. The time scale of the evolution is in the order of hundred years and perturbations typically migrate in the order of 10 meters per year. The mechanism responsible for the growth of perturbations is explained in terms of vorticity concepts. The alongshore gradient in the transfer of vorticity in the alongshore direction generates residual circulation cells that cause a growth of the perturbation. The cross-shore gradient in the transfer of vorticity in the cross-shore direction induces residual circulation cells that cause a decay of the perturbations. If the influence of waves on the net sediment transport is ignored, there is no fastest growing mode. When the wave-induced sediment transport is accounted for, the model predicts a fastest growing mode with wavelengths that can be in the order of observed length scales of barrier islands. The model predicts that the wavelength of the preferred mode decreases with increasing amplitude of the tidal currents and increases with increasing wave height. This is in gross correspondence with observed behavior of the lengths of barrier islands that are located along the Dutch and German Wadden coast and of those located in the Georgia Bight.

2.1   Introduction

A large part of the world's sandy coastlines show alongshore rhythmic variations on a wide range of length and time scales (*Ehlers*, 1988; *Komar*, 1998; *Ruessink and Jeuken*, 2002). This chapter focuses on rhythmic mesoscale variations of sandy coasts, i.e., with a characteristic length scale in the alongshore direction of a few kilometers to tens of kilometers. Such mesoscale variations are e.g. observed along the Dutch, German and Danish Wadden coast. This coast is characterized by a sequence of barrier islands and inlets. The typical length of the barrier islands decreases from a maximum length of 30 km for the island of Texel to an absence of barrier island in the German Bight (see Figure 1.6). It has been noted that the typical length of the barrier islands is inversely related to the tidal range (*Oost and de Boer*, 1994). The tidal range increases when moving from the Dutch part of the Wadden Sea to the Danish part, as has been discussed in Chapter 1. This behavior of the length of barrier islands along the Dutch and German Wadden Sea is not unique. In the Georgia Bight a similar relation between tidal range and the length of the barrier islands is observed (*FitzGerald*, 1996). In addition, the length of the barrier islands in this region is also linearly related to the mean height of the waves (see Chapter 1 for more details).

The general objectives of the present study are twofold. The first is to gain fundamental knowledge about the origin of the observed rhythmic mesoscale variations of the coastline using a model. The second is to derive a qualitative relationship between the characteristic length of these undulations and physical control parameters (like tidal, wave and shelf characteristics). In the past, several models were developed to study the dynamics of coastlines which are influenced by waves. They are all one-line models, i.e., the complex three-dimensional dynamics is parameterized, resulting in an equation for the coastline position only. A simple, widely used one-line model that simulates the initial evolution of rhythmic alongshore perturbations of a straight coastline, is that described by *Komar* (1998) (originally from *Pelnard-Considère* (1956)). In this model it is assumed that the width of the surf zone (the area where the waves are breaking) is constant. The conceptual idea is that obliquely incident waves refract and break in the surf zone and drive a current which transports sediment. Alongshore variations in this sediment transport result in changes of the position of the coastline. Under the aforementioned assumptions, and by only considering the dynamics due to a small rhythmic perturbation of the coastline, the *Komar* (1998) model boils down to a diffusion equation for the position of the coastline. The diffusion parameter is a function of the wave characteristics at the breaker line and the angle between the direction of the wave rays at breaking and the normal of the local (perturbed) coastline. A positive diffusion parameter implies that a small initial perturbation of the coastline will decay and a negative diffusion parameter results in growth. A negative diffusion parameter is obtained when the angle between wave rays at breaking and the normal of the local coastline is more than 45 degrees.

The one-line model of *Komar* (1998) was extended by *Ashton et al.* (2001); *Falqués* (2003). They assumed that a change in the position of the coastline also results in a change of the bathymetry outside the surf zone. The bathymetric contour lines are kept parallel. Hence, a change in the position of the coastline results in a shift of the entire bayhymetric profile. Already far offshore the waves are influenced by the change in the coastline

position because the bottom has changed. The diffusion parameter is now calculated as a function of the wave characteristics far offshore. The model results of *Falqués* (2003) show that the diffusion parameter in the model of *Komar* (1998) is always positive because the waves refract such that the wave rays at breaking will always have an angle of less than 45 degrees with respect to the normal of the local coastline. This does not imply that in the model of *Falqués* (2003) the perturbations of the coastline always decay. The model also takes into account the influence of alongshore variations in the wave height at the breaker line due to focusing of wave energy. Adding this effect leads to the so-called high-angle wave instability. Wave rays at deep water which have an angle of more than $42°$ with respect to the normal of the local coastline can lead to a growth of the perturbation of the position of the coastline.

Although interesting results are obtained with the models of *Ashton et al.* (2001) and *Falqués* (2003), there are problems with the physical interpretation. The main problem is that in these models sediment mass is not conserved. In *Falqués and Calvete* (2005) this problem was solved. They assumed that a perturbation in the position of the coastline results in a perturbation of the bottom profile with finite cross-shore extent. Hence, the bathymetric contours far offshore are not parallel anymore to the bathymetric contour lines in the nearshore zone. The model results show that fastest growing modes emerge which have typical time scales of years and wavelengths of the order of 10 km. The model was applied to the Dutch coastline, where a sequence of barrier islands is observed. Using their model, the Dutch coastline was found to be stable, i.e., no growing rhythmic coastline undulations were found (*Ashton et al.*, 2003; *Falqués and Calvete*, 2005; *Falqués*, 2005).

Since the action of waves in itself is not sufficient to trigger the evolution of an undulating coastline along the Dutch and German Wadden coast, tidal motions might be important as well. The observation that the barrier length increases with decreasing tidal range seems to support the importance of tidal motion for understanding the emergence of coastline undulations. Therefore, in this study a process-based one-line model is developed and analyzed to study whether the feedback between the coastline and tidal currents can cause the initial formation of an undulating coastline with length scales ranging between a few and tens of kilometers. In section 2.2 a model is formulated in which coastline undulations develop as free instabilities of an alongshore uniform coastline. The new aspect of this model is that it explicitly accounts for the influence of tidal currents on the stability of the coastline. In section 2.3 the basic state is described and the linear stability analysis is discussed. The model calculates the growth rate and phase speed of the coastline perturbation for different alongshore wavelengths of the perturbation. The results of this linear stability analysis are presented in section 2.4. In section 2.5 the results are compared with observations. Section 2.6 gives the physical interpretation of the results, and in section 2.7 the results are discussed and the main conclusions are given.

2.2   Model formulation

In this study a Cartesian coordinate system is adopted with the x-axis pointing in the cross-shore direction, the y-axis coinciding with the alongshore mean position of the coast-

line and the z-axis pointing in the upward vertical direction. The domain of the model consists of three regions: the surf zone, the nearshore zone and the inner shelf (Figure 2.1(a)). The surf zone is the area where the waves break and is located between the coastline $x = x_c$ and the breaker line $x = x_b$. The nearshore zone is also called the active zone and is the area where bottom changes occur due to changes in the position of the coastline. The nearshore zone is located between the coastline $x = x_c$ and the transition line $x = x_t$, with $x_t > x_b$. Here, the transition from the nearshore zone to the inner shelf occurs. The inner shelf is the region that is located between the nearshore region and the outer shelf. Sediment transport is small and the time scale of bathymetric changes is large compared to that of the nearshore zone.

(a)   (b)
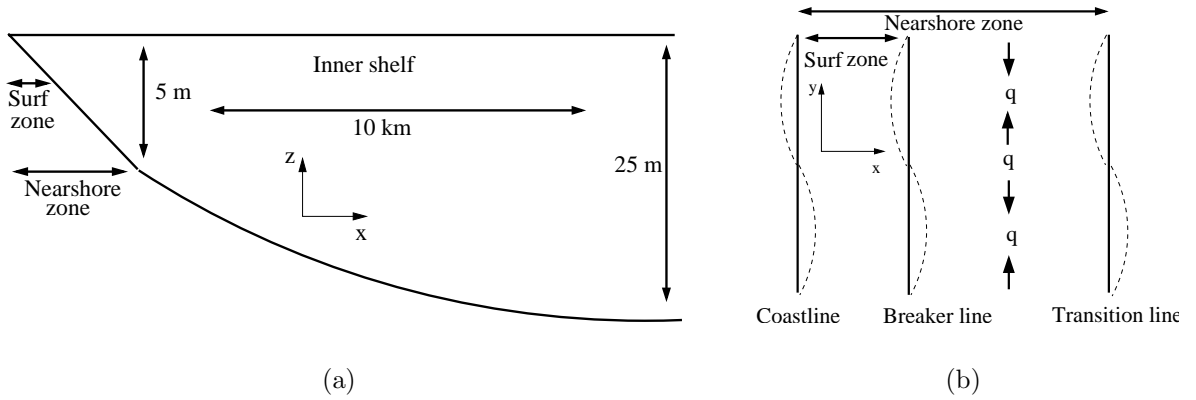
Figure 2.1: (a) Sideview of the geometry of the model. The nearshore zone is the area from the coastline to the transition line. The width of the nearshore zone is approximately 500 m. The surf zone is the area from the coastline to the breaker line. It has a width of typically 100 m. The transition between nearshore zone and inner shelf takes place at a typical depth of 5 m. The typical width of the inner shelf is 10 km. At the position where the inner shelf connects to the outer shelf the typical depth is 25 m. For more information see the text.
(b) Top view of the model. The position of the coastline is perturbed rhythmically and is denoted by the dashed variations. It is assumed that the width of the surf zone and the nearshore zone is constant. Therefore, the position of the breaker line and the position of the transition line are also perturbed when the coastline is perturbed. The typical length of the rhythmic variations of the position of the coastline is $1 - 10$ km. The volumetric sediment flux in the alongshore direction is denoted by q and takes place in the whole nearshore zone.

2.2.1 Hydrodynamics

The tidal hydrodynamics at the inner shelf are governed by the depth-averaged, shallow water equations. The water motion is forced by the semi-diurnal lunar (M_2) tide, which has frequency $\sigma \sim 1.4 \times 10^{-4}$ s^{-1}. The characteristic tidal wavelength is $L_g \sim 2\pi\sqrt{gH_*}/\sigma \sim$ 450 km, where g is the acceleration due to gravity and a $H_* = 10$ m a characteristic water depth. The spatial scales of the phenomena that are the focus of this study (typically $L_{barrier} \sim 10$ km) are small compared to the wavelength of the tidal wave. Hence, the Froude number (Fr $\sim L_{barrier}/L_g$) is very small. This allows for a rigid

lid approximation: The sea level variations themselves can be neglected, but their spatial gradients are important and result in pressure gradients in the momentum equations (see e.g., *Huthnance* (1982); *Calvete et al.* (2001)). The hydrodynamic equations are

$$\frac{\partial \vec{u}}{\partial t} + (\vec{u} \cdot \vec{\nabla})\vec{u} + f\vec{e}_z \times \vec{u} = -g\vec{\nabla}\zeta - \frac{\vec{\tau}_b}{\rho H} \tag{2.1a}$$

$$\vec{\nabla} \cdot \left(H\vec{u} \right) = 0 \tag{2.1b}$$

Here $\vec{u}$ is the horizontal velocity vector, t is time, $\vec{\nabla}$ the horizontal gradient operator, f the Coriolis parameter, $\vec{e}_z$ the unity vector in vertical direction, ζ the elevation of the free surface, H the water depth with respect to $z = 0$ and $\vec{\tau}_b$ the bed shear-stress. Usually, the bed shear-stress is taken to depend quadratically on the local velocity. In this study a linearized bed shear-stress formulation is used. Hence, instead of using

$$\vec{\tau}_b = \rho C_d |\vec{u}| \vec{u} \tag{2.2}$$

the bed shear-stress is approximated by

$$\vec{\tau}_b = \rho r \vec{u} \tag{2.3}$$

The friction factor r is taken such that the tidally averaged dissipation due to the linearized bottom stress equals that of the quadratic bottom stress. A discussion on the derivation of the linearized bed shear-stress can be found in *Zimmerman* (1992). In this study we choose the friction parameter to be

$$r = \frac{8}{3\pi} C_d U \tag{2.4}$$

with U the mean tidal velocity amplitude at the transition line. This implies that the friction parameter r is constant in the domain.

In this model tidal motion is due to a prescribed alongshore pressure gradient. As boundary conditions in the alongshore direction periodic conditions (with an as yet unspecified length scale) are imposed, at the transitions line the shore-normal velocity component must vanish and far offshore the velocity is required to have no cross-shore component:

$$x = x_t : \qquad u = v\frac{\partial x_t}{\partial y} \tag{2.5a}$$

$$x \to \infty : \qquad u \to 0 \tag{2.5b}$$

where u, v are the cross-shore and alongshore component of the velocity vector $\vec{u}$, respectively.

2.2.2   Volumetric sediment transport

The tidal hydrodynamics and sediment transport in the nearshore zone are not explicitly calculated in the model. Instead, the tidal currents are calculated on the inner shelf and the velocities at the transition line are taken as representative for the whole nearshore zone. They are used to calculate the volumetric sediment flux q in the nearshore zone (Figure 2.1(b)). In general, the sediment flux has a component due to waves and due to tides,

$$q = q_{(\text{wave})} + q_{(\text{curr})} \tag{2.6}$$

where $q_{(\text{wave})}$ is the part due to waves only and $q_{(\text{curr})}$ due to the joint action of tides and waves. It is assumed that $q_{(\text{curr})}$ involves the stirring of sediment form the bed by waves, which is subsequently transported by a tide-driven residual current. This is parameterized as

$$q_{(\text{curr})} = \beta < v_\parallel > \tag{2.7}$$

Here β is a constant and $< v_\parallel >$ is the tidally averaged shore-parallel component of the velocity at the transition line,

$$< v_\parallel > = \frac{1}{T} \int\limits_0^T v_\parallel dt \tag{2.8}$$

where T is the tidal period. The constant β in equation (2.7) accounts for the fact that the sediment is transported in the complete nearshore zone and has the unit of m^2. A physical interpretation of β is the available volume of sediment in the nearshore zone per unit length,

$$\beta = \int \int \frac{c}{\rho_s} dz dx \tag{2.9}$$

In this expression is c the tidally averaged sediment mass concentration and ρ_s the density of the sediment. The mean wave height along the Dutch and German Wadden coast is in the order of 1 m *Sha* (1989a). Using observations performed by *Grasmeijer and Kleinhans* (2004) of sediment concentrations at different levels in the vertical in the nearshore zone near Egmond aan Zee (the Netherlands) yields an estimate of $\int \frac{c}{\rho} dz = \mathcal{O}(5 \cdot 10^{-5} - 1 \cdot 10^{-3})$ m^3/m^2. Assuming that the width of the nearshore zone is in the order of 500 m, this yields that $\beta = \mathcal{O}(2.5 \cdot 10^{-2} - 5 \cdot 10^{-1})$ m^2.

Although the focus in this study is on the sediment transport due to tidal currents, some experiments have been performed in which both sediment transport due to waves only and tidal currents are accounted for (section 2.4.4). The expressions of *Pelnard-Considère* (1956); *Komar* (1998) are used to parameterize wave-driven sediment transport,

$$q_{(\text{wave})} = \mu H_b^{2.5} \sin 2(\theta_b - \phi) \tag{2.10}$$

where $\mu \sim 0.1 - 0.2$ m$^{\frac{1}{2}}$s^{-1} is a constant of proportionality, H_b is the (rms) wave height of the waves at the breaker line and $\theta_b - \phi$ (see Figure 2.2) is the angle between the wave fronts at breaking and the local coastline. In the present model both H_b and θ_b are input parameters. The local angle between the coastline and the y-axis is defined as

$$\phi = \arctan\Big[\frac{\partial x_t/\partial y}{(1 + |\partial x_t/\partial y|^2)^{1/2}}\Big] \tag{2.11}$$
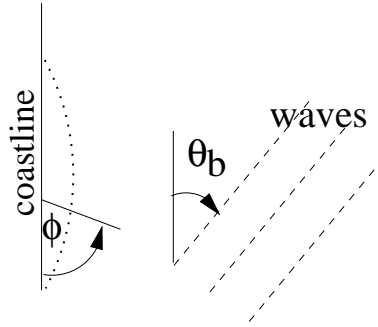
Figure 2.2: Definition of angle between wave rays at breaking and the local coastline. Dashed lines represent wave rays. Dotted line is coastline perturbation. The angle between y-axis and local normal to the coastline is ϕ and θ is the angle between the wave rays and the local unperturbed coastline.

2.2.3   Evolution of the coastline

When the position of the coastline changes, it can be expected that the bathymetry further offshore also changes. Hence, a change in the position of the coastline results in change of the position of breaker line and of the transition line. The most simple approach is to assume that variations in the coastline results in variations of the position of transition line of the same amplitude and vice versa, $x_t - x_c =$ constant. In this section the sediment mass balance is used to derive an evolution equation for the location of the transition line (x_t). Assume that the location of the coastline is shifted in time Δt over a small distance Δx_t (Figure 2.3). In the present model it is assumed that entire bathymetric profile in the nearshore zone shifts over a distance Δx_t. Therefore, the volume of sediment per unit length necessary for the displacement equals $\Delta x_t H(x = x_t) + \mathcal{O}(\Delta x_t^2)$. Here $H(x = x_t)$ is the depth at the transition line $x = x_t$. The change in the volume of sediment results from the convergence of the sediment transport in the alongshore direction, $\Delta q/\Delta y$. Taking the limit $\Delta q, \Delta x_t, \Delta y \to 0$, it follows that

$$\frac{\partial x_t}{\partial t} = -\frac{1}{H}\frac{\partial q}{\partial y}\Big|_{x=x_t} \tag{2.12}$$

The evolution of the transition line (and hence the coastline) takes place on a long morphological time scale T_m. Applying a scaling analysis and calculating the influence of alongshore variations in $q_{(\text{curr})}$ (Equation (2.7)) on the evolution of the coastline (defined
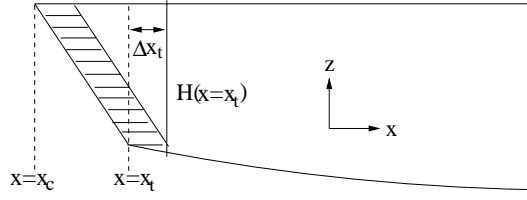
Figure 2.3: Sediment conservation in the present model. The coastline is at $x = x_c$ and the transition line at $x = x_t$. The coastline is shifted in seaward direction with Δx_t while $x_t - x_c$ is constant. The shaded area is the volume of sediment per unit length that is added to this coastal section.

by Equation (2.12)) and using boundary condition (2.5a) to obtain an estimate of $v_{\parallel}$ yields

$$T_m = \frac{[H(x = x_t)][\lambda]^2}{\beta[v]} \tag{2.13}$$

where the typical value of the alongshore tidal currents is $[v] = 1 \text{ ms}^{-1}$, the typical value of the alongshore wavelength of the perturbation is $[\lambda] = 10$ km, the typical depth at the transition line is $[H(x = x_t)] = 5$ m and typically $\beta = 10^{-1} \text{ m}^2$. Using these values, the morphological time scale is approximately 150 years. Physically this means that the coastline is not changing on the tidal time scale, but only on a very long time scale. Therefore, the position of the coastline can be considered as constant during one tidal cycle.

2.3   Basic state and linear stability analysis

2.3.1   Basic state

The model solutions are denoted by a state vector $\Psi = (\vec{u}, \vec{\nabla}\zeta, q, q_{(curr)}, q_{(wave)}, x_t)^T$. This state vector can be split into a part which describes a basic state with alongshore uniform conditions and a part which describes deviations from this basic state, $\Psi = \Psi_{eq} + \Psi'$. Here, $\Psi_{eq} = (\vec{U}, \vec{\nabla}Z, Q, Q_{(curr)}, Q_{(wave)}, X_t)^T$ with $\vec{U} = (U, V)$ the basic state velocity vector with components U and V in the x- and y-direction, respectively, and $\vec{\nabla}Z$ the basic state gradient of the sea surface. Furthermore, Q is the basic state volumetric sediment flux in the nearshore zone, $Q_{(curr)}$ and $Q_{(wave)}$ are the basic state volumetric sediment flux in the nearshore zone due to joint action of waves and tides and due to waves only, respectively, and X_t = constant is the position of the transition line in the basic state (straight coast).

In the basic state a spatially uniform alongshore pressure gradient is prescribed that consists of a residual component (S_0) and the main tidal (M_2) component with amplitude S_2 and frequency σ,

$$\frac{\partial Z}{\partial y} = -S_2 \cos \sigma t + S_0 \tag{2.14a}$$

$$\frac{\partial Z}{\partial x} = \frac{f}{g} V(x,t) \tag{2.14b}$$

No higher harmonics of the tide are taken into account. The free surface elevation Z is linear in the alongshore direction. In the cross-shore direction the gradient in the free surface elevation follows from geostrophic balance. The basic state velocity has an alongshore component that varies only in the cross-shore direction, i.e., $\vec{U} = (0, V(x,t))$. This velocity component is determined by a balance between inertia, alongshore sea surface gradient and depth-dependent friction,

$$\frac{\partial V}{\partial t} = -g\frac{\partial Z}{\partial y} - r\frac{V}{H} \tag{2.15}$$

The solution for the basic state velocity is

$$V(x,t) = V_2(x) \cos\left(\sigma t + \Phi(x)\right) + V_0(x) \tag{2.16}$$

with

$$V_2(x) = \frac{HS_2 g}{\sqrt{\sigma^2 H^2 + r^2}} \tag{2.17a}$$

$$V_0(x) = \frac{-gS_0}{r} H \tag{2.17b}$$

$$\Phi(x) = \arctan\left(\frac{r}{\sigma H}\right) \tag{2.17c}$$

The depth-dependent friction term in the alongshore momentum balance causes a phase lag between currents and sea surface gradient (in case of time dependent pressure gradient). It also results in an increasing magnitude of the alongshore velocity with increasing depth, i.e., cross-shore distance. Hence, the basic state velocity contains vorticity, defined by $\Omega(x,t) = \partial V(x,t)/\partial x$. Furthermore, the magnitude of U can be defined

$$U = V_2(x = X_t) \tag{2.18}$$

The basic state sediment transport due to tides is

$$Q_{(\mathrm{curr})} = \beta V_0 \tag{2.19}$$

Following *Komar* (1998), the basic state sediment transport that is solely due to waves reads

$$Q_{(\mathrm{wave})} = \mu H_b^{2.5} \sin\left(2\theta_b\right) \tag{2.20}$$

2.3.2   Stability analysis

The stability of the alongshore uniform coastline is studied by considering the dynamics of alongshore rhythmic perturbations. Hence, in Equations (2.1) and (2.4)-(2.12) $\Psi = \Psi_{eq} + \Psi'$ is substituted, with Ψ_{eq} as defined in Equations (2.14), (2.16), (2.19), (2.20), and $\Psi' = (\vec{u}', \vec{\nabla}\zeta', q', q'_{(curr)}, q'_{(wave)}, x'_t)^T$ denotes the state vector with the perturbed variables, which are assumed to be small compared to their values in the equilibrium state.

Linearizing the equations with respect to the small variables results in the following equations that describe the perturbed hydrodynamics,

$$\frac{\partial u'}{\partial t} + V\frac{\partial u'}{\partial y} - fv' = -g\frac{\partial \zeta'}{\partial x} - \frac{ru'}{H} \tag{2.21a}$$

$$\frac{\partial v'}{\partial t} + \left(u'\frac{\partial V}{\partial x} + V\frac{\partial v'}{\partial y}\right) + fu' = -g\frac{\partial \zeta'}{\partial y} - \frac{rv'}{H} \tag{2.21b}$$

$$u'\frac{dH}{dx} + H\frac{\partial u'}{\partial x} + H\frac{\partial v'}{\partial y} = 0 \tag{2.21c}$$

The linearized boundary conditions (2.5) read

$$u'\big|_{x=X_t+x'_t} = V\frac{\partial x'_t}{\partial y}\Big|_{x=X_t} \tag{2.22a}$$

$$u' = 0\big|_{x\to\infty} \tag{2.22b}$$

The next step is to find $q'_{(curr)}$ and $q'_{(wave)}$. Using (2.7) and the definition $v_\parallel = \vec{u} \cdot \vec{s}$, with $\vec{s}$ the tangent of the transition line, the tidally induced sediment transport at the undulating transition line becomes

$$Q_{(curr)} + q'_{(curr)} = \frac{\beta <V+v'>}{\left[1 + \left(\frac{\partial x'_t}{\partial y}\right)^2\right]^{1/2}}\Bigg|_{x=X_t+x'_t} \tag{2.23}$$

To evaluate this expression at location $x = X_t + x'_t$ (which is unknown), a Taylor expansion of the various variables is made, resulting in

$$Q_{(curr)} + q'_{(curr)} = \frac{\beta <V+v'> \big|_{x=X_t} + \beta x'_t \frac{\partial <V+v'>}{\partial x}\big|_{x=X_t} + \cdots}{1 + \frac{1}{2}\left(\frac{\partial x'_t}{\partial y}\right)^2 + \cdots} \tag{2.24}$$

Keeping only contributions that are linear in the perturbed quantities results in

$$q'_{(curr)} = \beta\left[<v'> + x'_t\frac{d<V_0>}{dx}\right]_{x=X_t} \tag{2.25}$$

For the perturbed wave-induced volumetric sediment flux $q'_{(wave)}$ the expression of *Komar* (1998) is used,

$$q'_{(wave)} = \mu H_b^{2.5}\cos(2\theta_b)\frac{\partial x'_t}{\partial y} \tag{2.26}$$

The last step is to obtain the evolution equation for the perturbed position of the transition line. The spatial variations in the sediment transport result in changes in the position of the coastline and the transition line. The linearized evolution equation for the position of the transition line becomes

$$\frac{\partial x'_{\mathrm{t}}}{\partial t} = -\frac{\beta}{H}\frac{\partial}{\partial y}\Big[<v'> + x'_{\mathrm{t}}\frac{d}{dx} <V_0> \Big]\Big|_{x=X_{\mathrm{t}}} + \gamma\frac{\partial^2 x'_{\mathrm{t}}}{\partial y^2} \tag{2.27}$$

Equation (2.27) clearly shows that the waves cause diffusion of the coastline perturbation with the diffusion parameter γ defined by

$$\gamma = \frac{2\mu H_b^{2.5}}{H(x=X_{\mathrm{t}})}\cos(2\theta_b) \tag{2.28}$$

2.3.3 Solution procedure

The model equations have solutions of the form

$$\Psi' = \Re\Big[\big(\hat{u}(x,t),\hat{v}(x,t),\vec{\nabla}\hat{\zeta}(x,t),\hat{q},\hat{q}_{(\mathrm{curr})},\hat{q}_{(\mathrm{wave})},\hat{x}_t\big)e^{iky}e^{\Gamma t}\Big]^T \tag{2.29}$$

Note that all variables behave exponentially in time. Besides, the hydrodynamic variables also show oscillatory behaviour on the tidal time scale which is much smaller than the time scale on which the transition line is evolving. The alongshore wave number is denoted by k and can be chosen arbitrarily. Furthermore, $\Gamma = \Gamma_{\mathrm{re}} + i\Gamma_{\mathrm{im}}$ is the complex growth rate, with a real part (Γ_{re}) that describes the growth of the perturbations, and an imaginary part (Γ_{im}) that determines the phase speed, $c = -\Gamma_{\mathrm{im}}/k$.

The aim is to determine $\hat{u}(x,t),\hat{v}(x,t),\vec{\nabla}\hat{\zeta}(x,t),\hat{q},\hat{q}_{(\mathrm{curr})},\hat{q}_{(\mathrm{wave})},\hat{x}_t$ and Γ as a function of wave number k and model parameters. The interest is in perturbations that have positive growth rates ($\Gamma_{\mathrm{re}} > 0$). The mode with wave number $k = k_p$ that has the largest growth rate will dominate the dynamics after some time. Therefore, it is called the most preferred mode. The growth rate is calculated as follows. First, the perturbation x'_{t} with given wave number k is chosen. The hydrodynamic problem, described by Equations (2.21a), (2.21b), (2.21c) and boundary conditions (2.22), has to be solved. Because the alongshore dependence of the variables is known a priori, $\hat{v}$ is known as a function of $\hat{u}$ (Equation (2.21c)), and reads

$$\hat{v} = -\frac{\hat{u}\frac{dH}{dx} + H\frac{\partial \hat{u}}{\partial x}}{ikH} \tag{2.30}$$

The two momentum equations (2.21a) and (2.21b) are combined into a vorticity equation. This is done by taking the x-derivative of Equation (2.21b) and subtracting the y-derivative of Equation (2.21a). When substituting for $\hat{v}$, one equation for the complex cross-shore velocity $\hat{u}$ is found,

$$U_{12}\frac{\partial^3 \hat{u}}{\partial t\partial x^2} + U_{11}\frac{\partial^2 \hat{u}}{\partial t\partial x} + U_{10}\frac{\partial \hat{u}}{\partial t} + U_{02}\frac{\partial^2 \hat{u}}{\partial x^2} + U_{01}\frac{\partial \hat{u}}{\partial x} + U_{00}\hat{u} = 0 \tag{2.31}$$

The coefficient U_{ij} are given in the appendix. As boundary conditions at $x = X_{\mathrm{t}}$ $\hat{u}$ is prescribed and for $x \to \infty$ it is required that $\hat{u} \to 0$. Solving Equation (2.31) together

with the boundary conditions yields $\hat{u}$, and using Equation (2.30) yields $\hat{v}$. Now, the perturbed sediment transport $\hat{q}_{\text{(curr)}}$ is known. For given wave conditions also $\hat{q}_{\text{(wave)}}$ can be calculated. Substituting Equation (2.29) into Equation (2.27) yields an expression for Γ,

$$\Gamma \hat{x}_t = -\frac{\beta}{H}\Big(ik < \hat{v} > +\hat{x}_t \frac{dV_0}{dx}\Big)\Big|_{x=X_{\text{t}}} -\gamma k^2 \hat{x}_t \tag{2.32}$$

2.3.4   Numerical implementation

Equation (2.31) is solved using a pseudospectral method. The spatial variables are expanded in Chebyshev polynomials (see *Boyd* (2001) for details). In previous morphodynamic modeling studies these Chebyshev polynomials have been successfully used in resolving spatial patterns (*Falqués et al.*, 1996). Employing the method discussed *Calvete et al.* (2001), for the time-dependent part a Galerkin approach is adopted. The velocity component $\hat{u}$ and $\hat{v}$ are expanded in their harmonic agents M_0, M_2, M_4 and so on. In this study the series is truncated after the M_2 components, so nonlinear tides are not accounted for. Hence, the variables are expanded as

$$\hat{u}(x,t) = \sum_{p=1}^{N}\Big[u_p^0 + u_p^{-1}e^{-i\sigma t} + u_p^1 e^{i\sigma t}\Big]T_i(\tilde{x}) \tag{2.33a}$$

$$\hat{v}(x,t) = \sum_{p=1}^{N}\Big[v_p^0 + v_p^{-1}e^{-i\sigma t} + v_p^1 e^{i\sigma t}\Big]T_i(\tilde{x}) \tag{2.33b}$$

$$\tag{2.33c}$$

where $x = L_x\frac{1+\tilde{x}}{1-\tilde{x}}$ with L_x is a stretching parameter and T_i are Chebyshev polynomials. Furthermore, N is the number of collocation points in the x-direction and u_p^0, u_p^{-1}, u_p^1 are the Chebyshev coefficients of the residual component, the $e^{-i\sigma t}$ Fourier component and the $e^{i\sigma t}$ Fourier component of the cross-shore velocity, respectively. The expansions of Equation (2.33) are substituted into Equation (2.31) and are evaluated at N collocation points in the x-direction. This results in a system of $3N$ by $3N$ linear algebraic equations with $3N$ variables of the form $Ax = B$, which is solved by standard numerical techniques. Here, A is a complex $3N$ by $3N$ matrix describing the model equations. The vector x describes the coefficients of the expansions of Equation (2.33). The complex vector B is zero for all 3N components, except for the collocation points at the transition line. In those points the magnitude of $\hat{u}$ is prescribed (boundary condition (2.22)).

2.4   Results

2.4.1   Reference case

In the first experiments the focus is on the influence of tidal currents on the stability of the equilibrium state with respect to perturbations in the position of the coastline.
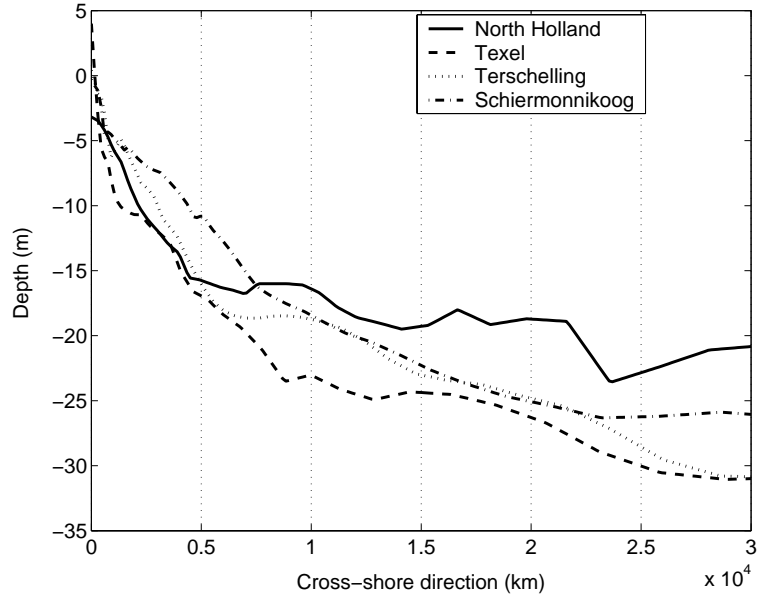
Figure 2.4:   Four cross-shore profiles along the Frisian Islands. The profile of 'North Holland' is taken 20 km south of Den Helder. For other positions of cross-shore transects, see Figure 1.6.

Thus, $\gamma = 0$ is assumed in Equations (2.27) and (2.32). Within the present model this situation occurs when the angle of wave incidence $\theta_b = 45°$. The meaning of this choice will be discussed later on. Experiments are performed for parameter values which are representative for the Dutch coastal area. The following profile has been used to represent the depth profile of the inner shelf,

$$H(x) = H_0 + (H_s - H_0)(1 - e^{-(x-X_t)/L}) \tag{2.34}$$

Here, $H_0 = H(x = x_t)$ and far offshore, where the inner shelf connects to the outer shelf, the depth is H_s. Parameter L is an e-folding length scale which is a measure of the width of the inner shelf. Typical values have been determined by fitting this expression to observed profiles along the Dutch coast. This yields estimates of $H_0 \sim \mathcal{O}(1 - 10)$ m, $H_s \sim \mathcal{O}(15 - 25)$ m and $L \sim \mathcal{O}(8 - 15)$ km. In the reference experiment $H_0 = 5$ m, $H_s = 20$ m and $L = 10$ km. The alongshore sea surface gradient is chosen such that the maximum velocity amplitude at the transition line is $V_2(x = X_t) = U = 0.5 \text{ ms}^{-1}$. No net flow is considered in the basic state ($S_0 = 0$). The Coriolis parameter $f = 1.14 \cdot 10^{-4} \text{ s}^{-1}$ and the drag coefficient $C_d = 2.5 \cdot 10^{-3}$. Furthermore, it has been used that $\beta = 10^{-1} \text{ m}^2$. The number of collocation points is $N = 100$ and the stretching parameter $L_x = 10$ km.

The dependence of the growth rate on the alongshore wave number is shown in Figure 2.5(a). The growth rate is scaled with T_m, so a growth rate of 1 corresponds to an e-folding time scale of 150 years. The variable along the horizontal axis of Figure 2.5(a) is the non-dimensional alongshore wave number $kL = 2\pi L/\lambda$, where λ is the wavelength and $L = 10$ km is the width of the inner shelf. The basic state is stable with respect to perturbations having small values of the dimensionless wave number, corresponding to wavelengths which are long compared to the width of the inner shelf. Perturbations with these wavelengths have negative growth rates and hence decay exponentially. For $kL > 3$

the growth rate increases with increasing kL and for $kL \sim 8$ the growth rate is zero. The wavelength of the perturbation with zero growth rate is called λ_0. In this case $\lambda_0 = 7.9$ km. For $kL > 8$ the growth rate is positive. Hence, there is a positive feedback between the coastline perturbation and the tidal flow. The growth rate curve does not show a maximum, so there is no fastest growing mode. For large wave numbers the growth rate tends to a constant.

The model also yields the phase speed of the perturbations. This phase speed is shown as a function of the dimensionless alongshore wave number in Figure 2.5(b). It has a minimum for $kL \sim 5$ and decreases for larger kL. A nondimensional phase speed of -0.3 is in dimensional values -20 m/yr. A negative sign means that the perturbation is migrating in the negative y-direction, that is to the right when viewing in the seaward direction.

(a)   (b)
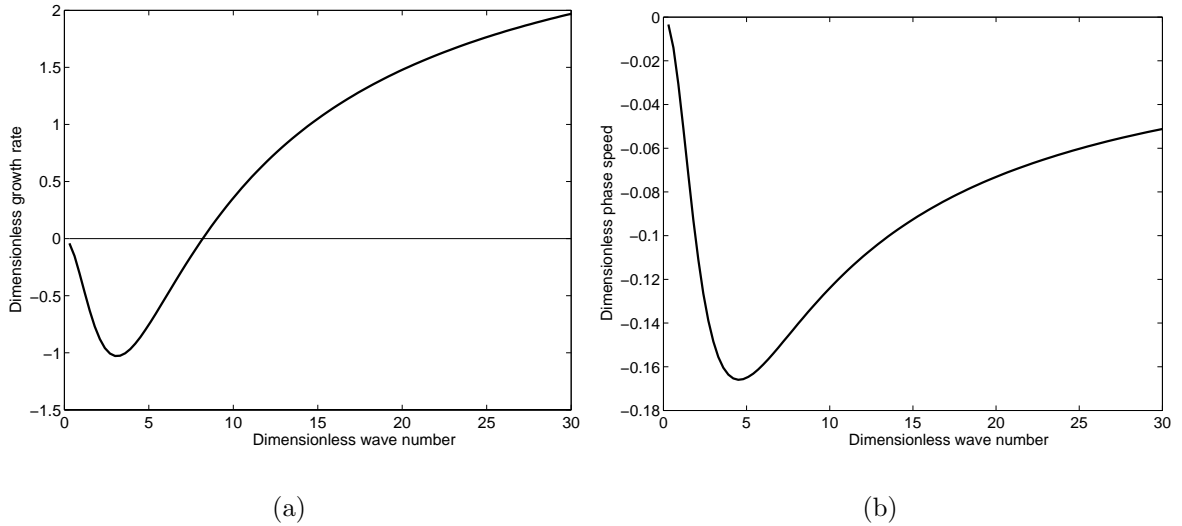
Figure 2.5: (a) Growth rate as a function of wave number for the reference case. A growth rate of 1 corresponds to an e-folding time scale of 150 years. Wave numbers are scaled with the width of the inner shelf, 10 km. (b) Phase speed as a function of wave number for the reference case. A phase speed of -0.3 corresponds to a dimensional phase speed of -20 m/yr.

The sediment transport $q'_{(curr)}$ is linear in the residual currents (Equation (2.25)). Figure 2.6(a) shows a vector plot of the residual currents on the inner shelf. Because the model does not yield a fastest growing mode, a wavelength is chosen that has a positive growth rate, $\lambda = 3$ km ($kL = 20.9$). Furthermore, because the the model is linear in x'_t an amplitude is chosen of $[x'_t] = 500$ m. Two residual circulation cells per alongshore wavelength appear. The structure of the residual circulation cells is such that the maximum convergence of the velocity at the transition line (and hence the convergence of the net sediment flux) is slightly out of phase (to the right when viewing in the seaward direction) with the coastline perturbation. The perturbation will therefore grow and migrate. The migration is forced by the Coriolis force. When $f = 0$, there is no phase difference between the residual velocities at the transition line and the coastline perturbation (Figure 2.6(b)). Hence, the perturbation does not migrate. The magnitude of the velocities is determined
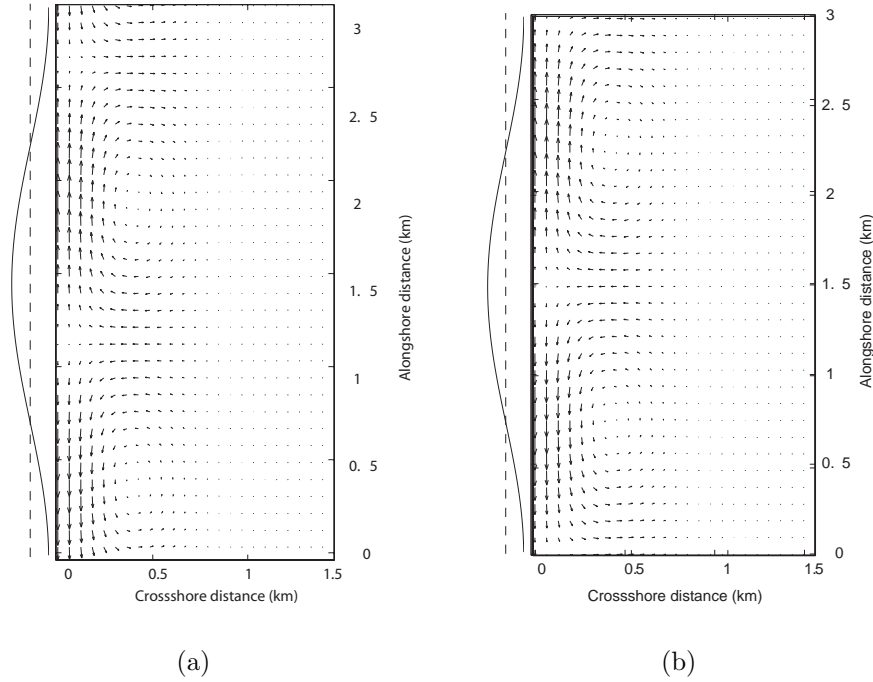
Figure 2.6: (a) Vector plot of residual currents for a perturbation of the coastline with alongshore wavelength $\lambda = 3$ km ;reference case. The coastline perturbation is shown at the left-hand side. An amplitude of the coastline perturbation of $[x'_t] = 500$ m has been chosen. This yields that $[<u'>] \sim [<v'>] = 10^{-2}$ ms^{-1}. The residual flow is such that the perturbation is amplified. In addition, the Coriolis force induces a migration of the perturbation.(b) Same as (a), but now the residual currents in the case of no Coriolis. In this case the coastline perturbation only grows and is not migrating.

by the amplitude of the coastline perturbation. This amplitude can be chosen arbitrarily.

2.4.2 Sensitivity of results to tidal current amplitude

Observations show that the shore-parallel tidal current amplitudes on the transition line vary between approximately 0.1 ms^{-1} and ~ 1 ms^{-1} in regions where barrier islands are observed. In the reference case the maximum tidal velocity at the transition line was 0.5 ms^{-1}. In the next experiment the magnitude of the basic state tidal velocity at the transition line is varied between 0.1 and 1.0 ms^{-1}. A change in the magnitude of the basic state velocity causes a change of the magnitude of the friction parameter r, defined in Equation (2.4). The friction parameter scales linearly in the magnitude of the tidal velocity. All other parameters have the same values as in the reference experiment.

The influence of the magnitude of the tidal currents at the transition line (U) on the growth rate is shown in Figure 2.7(a). Larger values of U result in larger growth rates for large kL. Furthermore, a larger velocity magnitude results in a larger λ_0. Hence, coastline perturbations with larger length scales grow exponentially in time. For $U = 0.1$ ms^{-1} $\lambda_0 = 4.6$ km, while for $U = 1$ ms^{-1} $\lambda_0 = 10.3$ km.

A change the magnitude of the tidal currents at the transition line (U) leads to only

a moderate change of the phase speed (Figure 2.7(b)). The plot reveals that a change in U will not influence the phase speed of the coastline perturbation for small wavelengths. For larger wavelengths the tidal current amplitude does influence the phase speed. A smaller tidal current results in a smaller phase speed. However, a doubling of the tidal current amplitude with respect to the reference experiment hardly affects the phase speed for small kL.

(a)   (b)
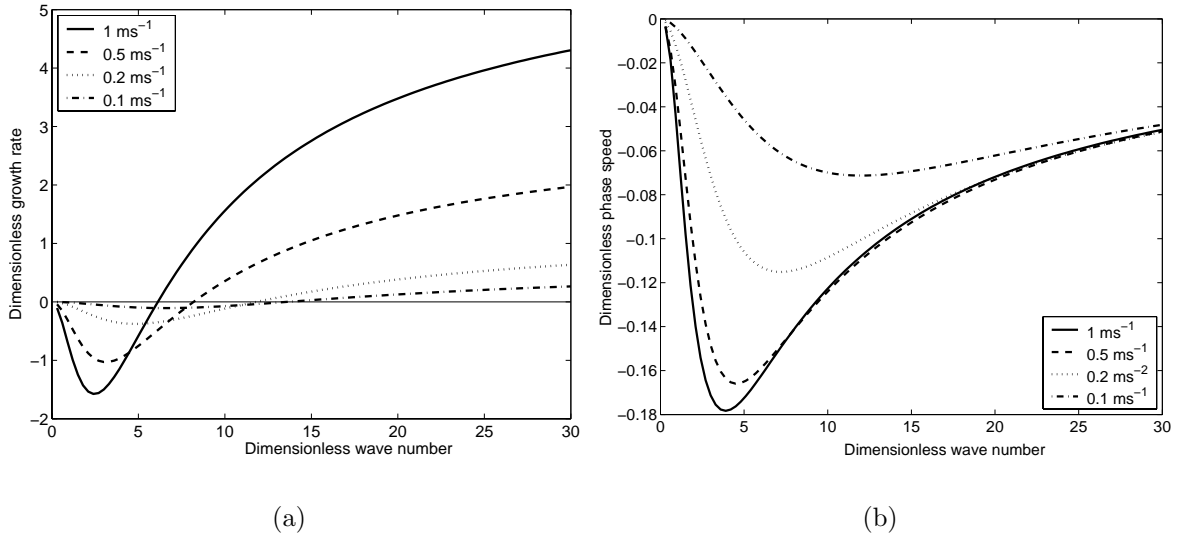
Figure 2.7: (a) Growth rate curves for different values of the magnitude of the basic state tidal M_2 flow at the transition line. The magnitude of U is 0.1, 0.2, 0.5 and 1.0 ms^{-1}, respectively. A dimensionless growth rate of 1 corresponds to time scale of 150 years and alongshore wave number is scaled with 10 km. (b) Same as (a), but now the phase speed as a function of the wave number. A non-dimensional phase speed of -0.3 is in dimensional values -20 m/yr.

In a second series of experiment, a time-invariant pressure gradient S_0 was prescribed. Hence, the basic state velocity has a residual component on top of the tidal component. The profile is described by Equation (2.17b). The residual pressure gradient is chosen such that $V_0(x = X_t)$ is varied between 0.02 and -0.02 ms^{-1}. This implies that the residual currents far offshore are varied between -0.1 and 0.1 ms^{-1} for the reference bathymetry. All other parameters have their reference values. Results are shown in Figure 2.8. Growth rates of perturbations of the coastline are hardly affected by this small basic state residual current. The phase speed, however, is strongly influenced by the basic state residual current. For $V_0(x = X_t) = -0.02$ ms^{-1} all perturbations are migrating to the right (when viewing in seaward direction). For smaller wavelengths (larger kL) the phase speed is larger. For $V_0(x = X_t) = 0.02$ ms^{-1} the perturbations are migrating to the right for $\lambda > 9.5$ km ($kL < 6.6$) and for $\lambda < 9.5$ km ($kL > 6.6$) the perturbations are migrating to the left.
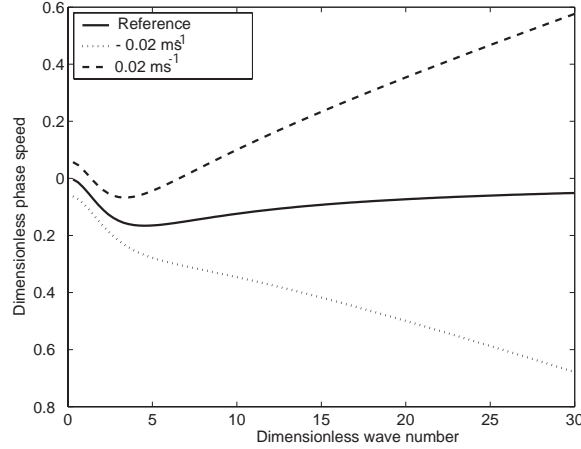
Figure 2.8:   Phase speed as a function of the wave number for different values of the residual current amplitude at the transition line ($V_0(x = X_t)$). Non-dimensional phase speed of -0.3 is -20 m/yr in dimensional values. Alongshore wave number is scaled with a length of 10 km.

2.4.3   Sensitivity of results to bathymetric parameters

The bathymetry of the inner shelf influences the basic state velocity profile. Therefore, in this section the sensitivity of the results to the bathymetric parameters (in particular L and H_0) is studied. In the first experiment the length of the inner shelf is varied with all other parameters having their reference values. Experiments show that a steeper profile results in smaller values of λ_0 (Figure 2.9(a)). The dependence of λ_0 on L is almost linear. Not only λ_0 changes, but also the growth rate. For small values of L, growth rates are larger for small wavelengths compared to the reference case. For relatively large values of L, growth rates are smaller for small wavelengths compared to the reference case. The sensitivity of the phase speed to L is shown in Figure 2.9(b). The magnitude of the phase speed is larger when L is smaller. For $L = 5$ km the phase speed has a maximum of 16 m/yr for $\lambda = 12.6$ km ($kL = 5$).

In another series of experiments the value of H_0 was changed. When H_0 is changed the value of β has to be changed as well. Parameter β can be interpreted as the volume per unit length in the alongshore direction of sediment that is in suspension in the nearshore zone (see Equation (2.9)). It is assumed that the steepness of the nearshore zone is constant and that the average concentration in the nearshore zone does not change with changing H_0. From this it follows that $\beta \sim H_0^2$. Furthermore, when H_0 is changed and the alongshore sea surface gradient S_2 is kept fixed, the magnitude of the friction parameter r should be changed as well. However, it is assumed that the profile of the basic state velocity is not changed, which implies that the velocity profile is such that the tidal current amplitude is 0.5 ms^{-1} at 5 meters depth. The friction parameter r and the amplitude of the M_2 pressure gradient S_2 keep their reference values.

The results of Figure 2.10(a) show that a smaller H_0 results in a shift of λ_0 to smaller wavelengths. For small wavelengths a smaller H_0 results in larger growth rates, compared to the reference case (Figure 2.10(a)). The influence of H_0 on the phase speed is shown in Figure 2.10(b). An increase of H_0 with respect to the reference experiment results in
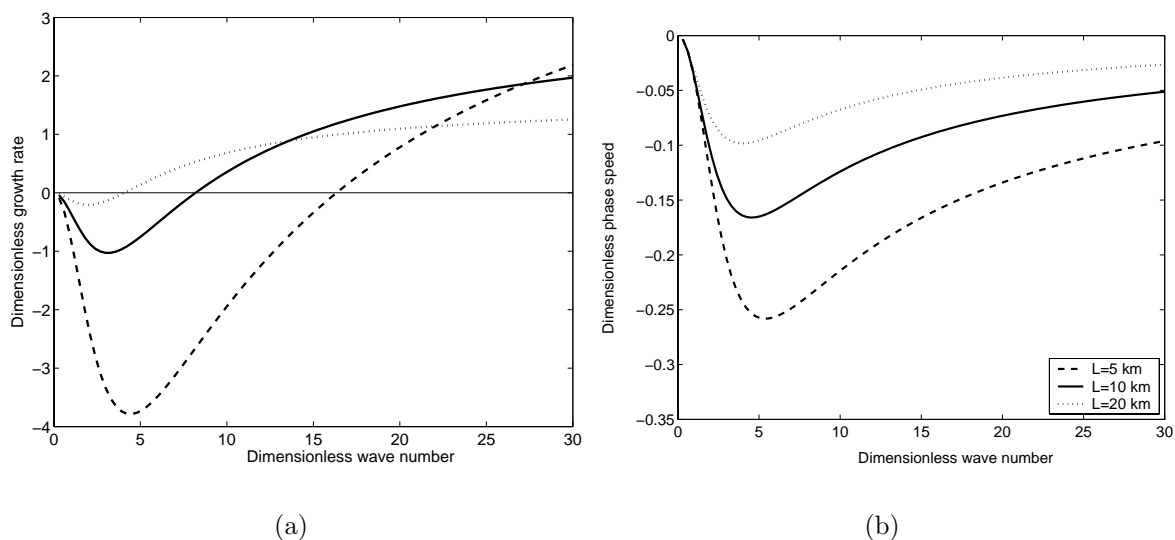
Figure 2.9: (a) Growth rate curves for $L = 5$ km (dashed line), $L = 10$ km (solid line) and $L = 20$ km (dotted line). A dimensionless growth rate of 1 corresponds to time scale of 150 years and alongshore wave number is scaled with 10 km. (b) Same as (a), but now the phase speed as a function of the wave number. A dimensionless phase speed of -0.3 corresponds to a dimensional phase speed of -20 m/yr.

an increase of the phase speed. A decrease of H_0 results in a decrease of the phase speed. The phase speed is in the order of 10 m/yr.
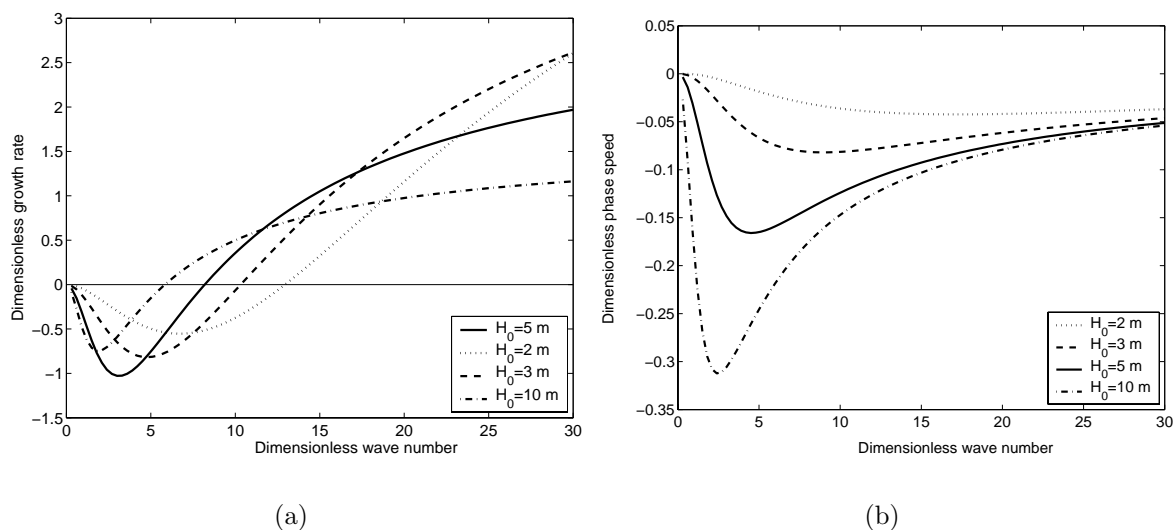
Figure 2.10: (a) Growth rate curves for different values of H_0. A dimensionless growth rate of 1 corresponds to time scale of 150 years and alongshore wave number is scaled with 10 km. (b) Same as (a), but now the phase speed as a function of the wave number. A dimensionless phase speed of -0.3 is in dimensional values -20 m/yr.

2.4.4 Influence of waves on the instability mechanism

In all the previous experiments, i.e. with significant tidal currents and $\gamma = 0$, no fastest growing mode was obtained. Hence, the model can not explain why undulations of the coastline have preferred length scales, as field data indicate. Furthermore, the growth rates are largest for the smallest wavelengths, which implies that perturbations with an infinitesimal small length scale will grow fastest. Hence, the model is missing a mechanism that results in decay of the perturbations with the smallest length scale. By accounting for a net volumetric sand flux due to obliquely incident waves ($q'_{(\text{wave})}$), a selection mechanism for the growing perturbations is introduced. In the model of *Komar* (1998) the divergence the sediment transport due to waves is modeled as a diffusive term and it causes a decay of the perturbations. This decay is fastest for the smallest length scales. In the next experiment the diffusivity of coastline perturbations due to waves is included. Two types of experiments are presented. In the first experiment the diffusion coefficient γ due to waves is constant while the magnitude of the alongshore tidal currents is varied. In the second experiment the magnitude of the alongshore tidal currents is constant and the value of θ_b is varied, thereby causing a change of diffusion coefficient γ (Equations (2.12) and (2.28)).

In all the previous experiments θ_b was 45°. This yielded that $q'_{(\text{wave})} = 0$. In the following experiments $H_b = 1$ m is taken and a different value for θ_b is assumed. In the first experiment the diffusion parameter is $\gamma = 2 \cdot 10^{-5}$ m^{2}s^{-1}, while other parameters settings are as in the reference experiment. This diffusion parameter is obtained for $H_b = 1$ m and $\theta_b = 44.94°$. Results show that a fastest growing mode occurs (Figure 2.11). For $U = 0.5$ ms^{-1} this occurs for $\lambda = 2.6$ km. The time scale on which these perturbation grow is 130 years. The perturbation migrates 5 meters per year. For $U = 0.8$ ms^{-1} a fastest growing mode is obtained at $\lambda = 2.26$ km, with a typical e-folding growth rate of 60 years. The phase speed is again 5 meters per year. For $U = 0.3$ ms^{-1} a fastest growing mode is obtained at $\lambda = 2.94$ km, with a typical e-folding growth rate of 470 years.

In the second experiment the shore-parallel tidal currents at the transition line are $U = 0.5$ ms^{-1}. All other parameters have their reference magnitude. The wave influence is varied by changing the magnitude of the diffusion parameter. The results show that for increasing wave influence and constant magnitude of the alongshore tidal currents, the preferred length scale of the undulations increases (Figure 2.12). The preferred length scale for $\gamma = 2 \cdot 10^{-5}$ m^{2}s^{-1} ($\theta_b = 44.94°$) is $\lambda = 2.6$ km and the corresponding time scale is 130 years. For $\gamma = 6 \cdot 10^{-5}$ m^{2}s^{-1} ($\theta_b = 44.83°$) a fastest growing mode is obtained for $\lambda = 3.6$ km, with a typical growth rate of 380 years. For $\gamma = 1 \cdot 10^{-4}$ m^{2}s^{-1} ($\theta_b = 44.71°$) the preferred wavelength is $\lambda = 4.8$ km (however, the growth rate is negative).

The fastest growing mode with the largest length scale is obtained for $H_0 = 10$ m, $H_s = 20$ m, $L = 20$ km, $U = 1$ ms^{-1} and $\gamma = 8 \cdot 10^{-4}$ m^{2}s^{-1} ($\theta_b = 40.42°$). In that case a fastest growing mode is obtained for $\lambda \sim 14$ km.

2.5 Comparison model results with observations

In this section the model results are compared with observations. The predicted dependence of the length scale of the fastest growing mode (FGM) on the magnitude of the tidal currents is compared with the observed trend along the Dutch and German Wadden
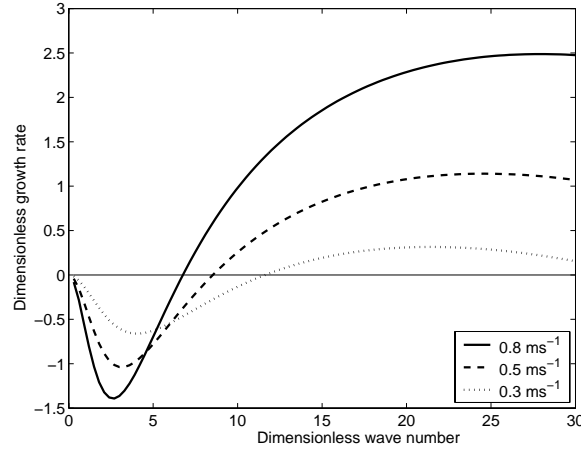
Figure 2.11:   Growth rate curves for constant values of the diffusion coefficient related to waves $(\gamma = 2 \cdot 10^{-5} \text{ m}^2\text{s}^{-1})$ and varying the magnitude of U.
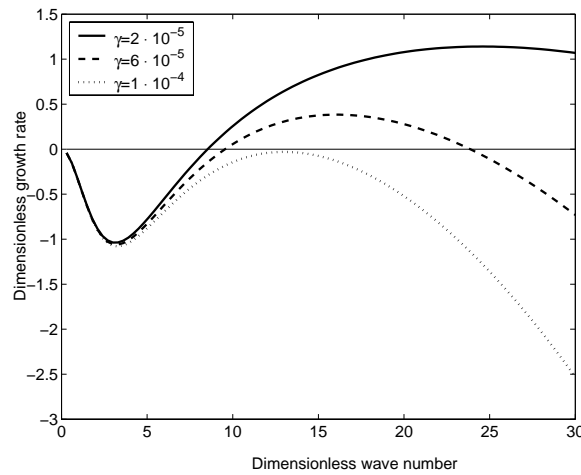
Figure 2.12:   Growth rate curves for different values of diffusion coefficient γ caused by waves and constant strength of tidal currents $(U = 0.5 \text{ ms}^{-1}$.

coast and in the Georgia Bight.

The length of the barrier islands along the Dutch and German Wadden Sea varies between a few kilometers (Simonszand and Rottumeroog) up to 30 kilometer (Texel) (*Ehlers*, 1988; *Oost and de Boer*, 1994). The typical migration speed of the islands is in the order of tens of meters per year and migration is from west to east *Luck* (1975). The length scales of the FGM obtained with the model have the correct order of magnitude. The typical length scale ranges from zero up to 15 kilometer. The predicted migration rates are also in accordance with the observed ones and vary between 5 and 24 meters per year, depending on the specific parameter values. The model also predicts that the perturbations are migrating to the east.

An important finding of the model is that the preferred length scale decreases with increasing magnitude of the tidal currents U. To test this result, observed wave and tidal characteristics along the Dutch and German Wadden coast were analyzed. It has

been argued by *Sha* (1989a) that the wave influence is constant along the Frisian Islands. Unfortunately, there are not many observations of the magnitude of the alongshore tidal currents at sea. Instead, the results of a numerical model were used. This is the ZUNO model from WL—Delft Hydraulics (*Roelvink et al.*, 2001), a model that has been developed to predict tidal heights and depth-averaged tidal currents in the southern North Sea. Figure 2.13(a) shows the major axis of the M_2 tidal current ellipse in the region of the Frisian Islands. The magnitude of the major axis in the regions close to the tidal inlets are strongly influenced by the dynamical interaction between the backbarrier basin and the ebb-tidal delta. Therefore, the magnitudes of the major axis far offshore are considered. It is assumed that these are representative for the situation that the coastline is straight and no tidal inlets are present. Two transects (see the two lines in Figure 2.13(a)) of the major axis of the M_2 tidal current ellipse are shown in Figure 2.13(b). These transects show that the long axis is increasing from Texel to Schiermonnikoog. Here the long axis has a maximum. From thereon it decreases when going to the island of Spiekeroog. The length of the barrier islands in this region is slightly larger than it is in the region just after Schiermonnikoog. The length scale of the barrier islands seems to be inversely related to the magnitude of the shore-parallel tidal currents. This is in agreement with model predictions.

(a)   (b)
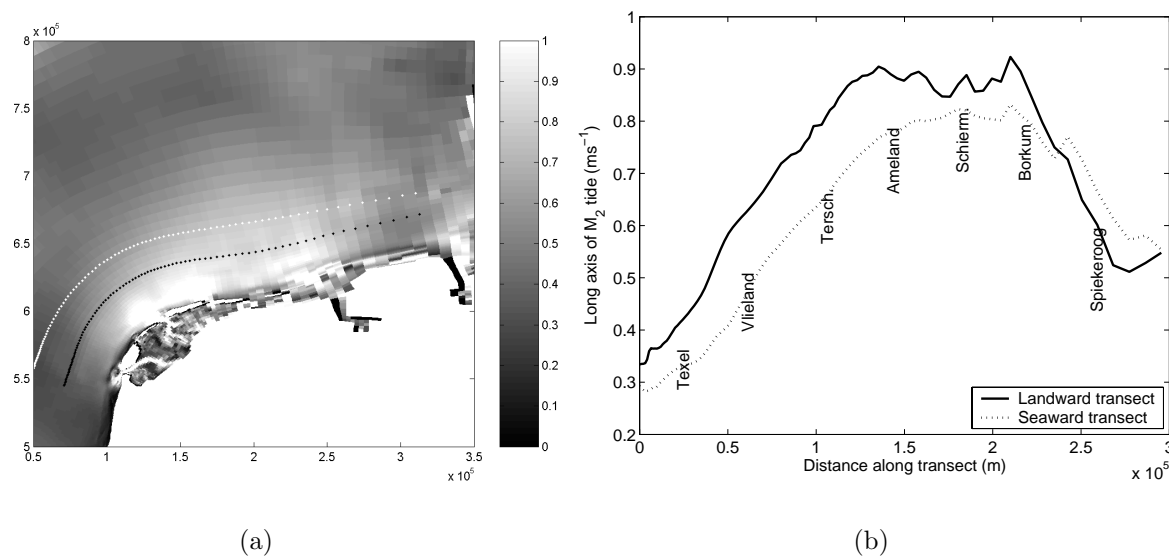
Figure 2.13: (a) Major axis of the M_2 tidal current ellipse in the region of the Frisian Islands. Model results are obtained with numerical model (ZUNO). White diamonds show seaward transect while black diamond show landward transect. (b) Two transects of the major axis of the M_2 tidal current ellipse in the region of the Frisian Islands. The two transects are shown in panel (a).

Finally, the model results are compared with observations in the Georgia Bight. In this area the magnitude of the tidal height and the tidal currents increases and wave influence decreases from the shelf of North Carolina towards the shelf of Georgia (*FitzGerald*, 1996; *Blanton et al.*, 2004). The model results predict that both the decreasing wave influence

and the increasing tidal current amplitude will result in smaller length scales of the barrier islands. This is in gross agreement with the observed trend in the length of the barrier islands in the Georgia Bight.

2.6   Physical interpretation

It was shown that for the default settings of the model parameters, perturbations with wavelengths $\lambda > 8$ km have negative growth rates, while for $\lambda < 8$ km the growth rate is positive. The perturbations not only grow but also migrate to the right when viewing in the seaward direction. When wave effects are included in the calculation of the alongshore sediment flux, a fastest growing mode is obtained. In this section these results are explained in terms of basic physical mechanisms. The following aspects are discussed:

- Why do perturbations decay for long wavelengths and grow for small ones?
- Why do perturbations migrate?
- Why are the growth rates small?
- What is the physical explanation behind sensitivity of the results to basic state bathymetry and velocity?

2.6.1   Growth and migration of perturbations

In this section the physical mechanism behind the growth and decay of the coastline perturbations is studied, with the focus on the role of tides in this process. The influence of wave-induced alongshore sediment fluxes on the evolution of perturbations of the coastline has already been discussed in *Komar* (1998).

The growth and migration of the perturbations are due to the divergence of the volumetric sediment flux $q'_{(\mathrm{curr})}$ as defined in Equation (2.25). This flux is linearly related to the tidally averaged velocity at the transition line, which is related to circulation patterns (see Figure 2.6(a) and 2.6(b)) on the inner shelf. The physics causing the generation of residual circulation cells will be analyzed using vorticity concepts in a similar way as described in *Zimmerman* (1981). The vorticity balance for the perturbed variables, retaining only linear terms, is obtained by taking the x-derivative of Equation (2.21b) and subtracting the y-derivative of Equation (2.21a):

$$\overbrace{\frac{\partial \omega'}{\partial t}}^{(a)} + \overbrace{\frac{\partial (u'\Omega)}{\partial x}}^{(b)} + \overbrace{\frac{\partial (V\omega')}{\partial y} + \frac{\partial (v'\Omega)}{\partial y}}^{(c)} - \overbrace{\frac{r}{H^2}\frac{dH}{dx}v'}^{(d)} + \overbrace{f\left(\frac{\partial u'}{\partial x} + \frac{\partial v'}{\partial y}\right)}^{(e)} = \overbrace{\frac{-r\omega'}{H}}^{(f)} \qquad (2.35)$$

Here, $\Omega = \partial V/\partial x$ is the vorticity of the basic state flow and $\omega' = \partial v'/\partial x - \partial u'/\partial y$ is the vorticity of the perturbed flow. In Equation (2.35), term (a) models the local time evolution of the perturbed vorticity, term (b) the cross-shore gradient of the perturbed vorticity flux in the cross-shore direction, term (c) the alongshore gradient of the perturbed vorticity flux in the alongshore direction, term (d) the generation of perturbed vorticity by the frictional torque, term (e) the generation of perturbed vorticity due to vortex stretching of the planetary vorticity and term (f) the dissipation of perturbed vorticity due to friction.

Generation of tidally averaged vorticity

Residual currents are organized in cells with cyclonic (anticyclonic) circulation. These cells are areas where the tidally averaged perturbed vorticity is positive (negative). To obtain the relation between the perturbation of the coastline and residual current at the transition line, it is thus important to study the tidally averaged vorticity balance. The latter follows from averaging Equation (2.35) over the tidal period and reads

$$\overbrace{-\left[\frac{\partial}{\partial x}\langle u'\Omega\rangle + \frac{\partial}{\partial y}\langle V\omega'\rangle + \frac{\partial}{\partial y}\langle v'\Omega\rangle\right]}^{1} + \overbrace{\frac{r}{H^2}\frac{dH}{dx}\langle v'\rangle}^{2} + \overbrace{\frac{f}{H}\frac{dH}{dx}\langle u'\rangle}^{3} = \overbrace{\frac{r}{H}\langle\omega'\rangle}^{4} \quad (2.36)$$

Here, $<>$ denotes an average over the tidal cycle, see Equation (2.8) for its definition. Also, the continuity equation (2.21c) has been applied here. The three source terms of tidally averaged vorticity are on the left-hand side of Equation (2.36). Term (1) describes the convergence of the tidally averaged perturbed vorticity flux, (2) the frictional torque due to alongshore currents over cross-shore sloping bathymetry and (3) the Coriolis torque due to vortex stretching. The right-hand side of Equation (2.36), term (4), describes the dissipation of residual perturbed vorticity due to friction.

Now, the different terms are estimated for a typical coastline perturbation of $\lambda = 3$ km, tidal currents at the transition line with a magnitude of $U = 0.5$ ms^{-1}, absence of residual currents at sea ($V_0(x = X_t) = 0$ ms^{-1}) and $f = 0$. The perturbation was already shown in Figure 2.6(b) . For this perturbation it turns out that the magnitude of term (2) is much smaller than that of term (1) because the generated residual currents are much smaller than the M_2 component of u' and v'. The main balance in Equation (2.36) is between the production of tidally averaged perturbed vorticity described by term (1) and the dissipation of it described by term (4).

So, to understand the generation of residual circulation cells the focus should be on term (1), which describes the gradient of three fluxes of vorticity. The first one is $< u'\Omega >$ and describes the mean flux of basic state vorticity by the perturbed cross-shore currents. The second one is $< \omega'V >$ and represents the mean flux of perturbed vorticity by the basic state alongshore currents. The third one is $< v'\Omega >$ and describes the mean flux of basic state vorticity by the perturbed alongshore currents.

Let us first consider the cross-shore gradient of $< u'\Omega >$. During flood the basic state tidal currents are in the negative y-direction: V_2 is negative, see Figure 2.14(a). Furthermore, $\partial V_2/\partial x < 0$ and therefore $\Omega < 0$. The perturbed cross-shore velocity u' during ebb is 180° out of phase phase with the alongshore gradient of the coastline perturbation (see Figure 2.14(a), which shows the perturbed velocity vector $\vec{u}'$). The vorticity flux $u'\Omega$ is therefore in phase with the alongshore gradient of the coastline perturbation. Because the magnitude of $u'\Omega$ is decreasing in the cross-shore direction, the cross-shore gradient of $u'\Omega$ during flood results in areas on the inner shelf where vorticity is accumulating with a same sign as that of the alongshore gradient of the coastline perturbation. During ebb the value of V_2, Ω and u' change sign. This results in the same sign of $u'\Omega$ and in the same cross-shore gradient of $u'\Omega$. Hence, the cross-shore gradient of the mean cross-shore vorticity flux results in areas on the inner shelf characterized by mean perturbed vorticity

which has the same sign as that of the alongshore gradient in the coastline perturbation. In other words, residual circulation cell as sketched in Figure 2.14(b) are generated. The mean currents transport the sediment from areas where the coastline has accreted to areas where the coastline has eroded. This results in a decay of the perturbation of the coastline.

Next, let us consider the alongshore gradient of $< v'\Omega >$ and $< V\omega' >$. During flood $V_2 < 0$ and $\Omega < 0$ (see above) and the perturbed alongshore velocity v' is $180°$ out of phase with the coastline perturbation (Figure 2.14(a)). The perturbed vorticity flux is $v'\Omega$ is therefore in phase with the coastline perturbation. The alongshore gradient of $v'\Omega$ is $180°$ out of phase with the alongshore gradient in the coastline perturbation and therefore leads to accumulation of vorticity with a sign that is opposite to that of the gradient of the coastline perturbation. This results in residual circulation cells as sketched in Figure 2.14(c). During ebb V_2, Ω and v' change sign. This results in the same sign of $v'\Omega$ and in the same alongshore gradient of $v'\Omega$. Hence, averaged over one tidal cycle the alongshore gradient of $v'\Omega$ results in mean perturbed vorticity with a sign opposite to that of the alongshore gradient in the coastline perturbation. The mean currents transport the sediment from areas where the coastline has eroded to areas where the coastline has accreted. This results in a growth of the perturbation of the coastline.

The last contribution to the convergence of the mean vorticity flux is the alongshore gradient of $< V\omega' >$. During flood, the perturbed vorticity ω' is in phase with the coastline perturbation of the coastline and the perturbed vorticity flux is $180°$ out of phase with the coastline perturbation because $V_2 < 0$. Hence, following a similar argumentation as for the alongshore gradient of $< v'\Omega >$, the alongshore gradient of $< V\omega' >$ results in residual circulation cells that cause a growth of the perturbation of the coastline.

Whether the residual circulation cells are located along the coast in such a way that the coastline perturbation is growing or decaying depends on the magnitudes of the cross-shore gradient of $< u'\Omega >$ and of the alongshore gradient of $< v'\Omega >$ and $< V\omega' >$. For small wave numbers the magnitude of the cross-shore gradient of $< u'\Omega >$ is larger than the alongshore gradient of $< v'\Omega > + < V\omega' >$ and therefore the locations of the residual circulation cells are such that the perturbations of the coastline decay. For increasing wave numbers the magnitude of the alongshore gradient of $< v'\Omega >$ and $< V\omega' >$ increases stronger than that the cross-shore gradient of $< u'\Omega >$. When the magnitude of the alongshore gradient of $< v'\Omega > + < V\omega' >$ is larger than the cross-shore gradient of $< u'\Omega >$, the locations of the generated residual circulation cells along the coast are such that the perturbations of the coastline grow.

When the Coriolis force is nonzero ($f \neq 0$) the perturbations also migrate. The Coriolis torque (term (e) in Equation (2.35)) is a source of tidal vorticity and causes a phase shift of the tidal vorticity with respect to the coastline perturbation. While in the case that $f = 0$ the perturbed vorticity ω' is in phase with the coastline perturbation during flood, in the case that $f \neq 0$ the maximum of the perturbed vorticity ω' is shifted in the negative y-direction with respect to the coastline perturbation due to planetary vortex stretching. The perturbed vorticity is transferred by the basic state velocity and the alongshore gradient of $V\omega'$ results in the accumulation of perturbed vorticity which is slightly shifted in the negative y-direction compared to the case that $f = 0$. During ebb a similar argumentation holds and residual circulation cells occur of which the centers are shifted
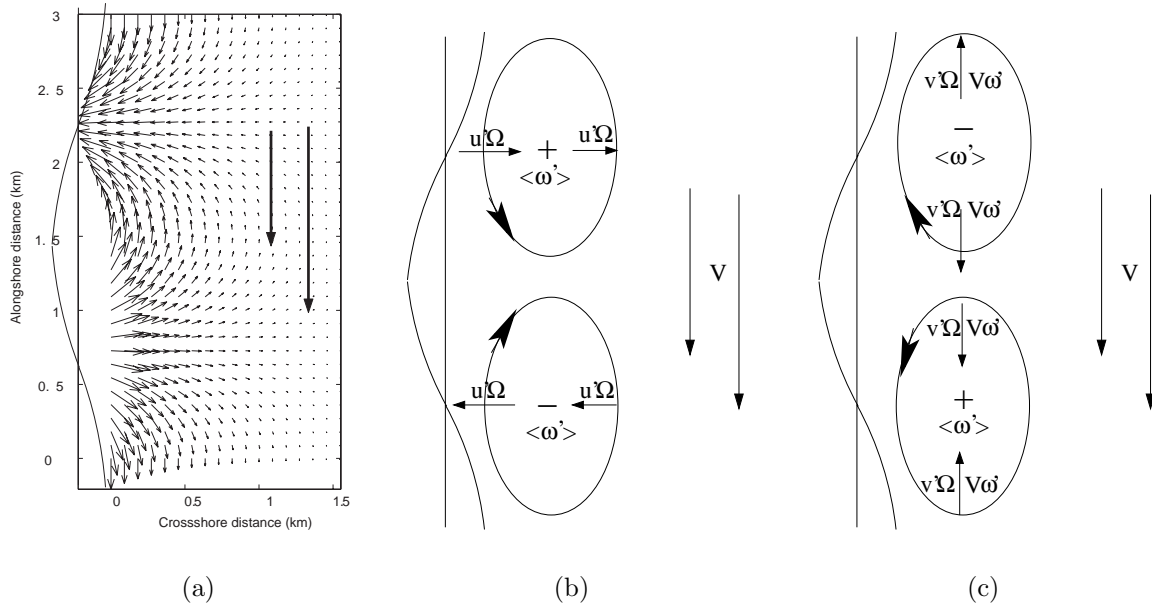
Figure 2.14: (a) Perturbed velocity induced by coastline at maximum flood. The basic tidal flow is from north to south (big arrows). The coastline perturbation has a cosine structure. (b) Small arrows represent perturbed cross-shore vorticity flux $u'\Omega$. The cross-shore gradient of the vorticity in the cross-shore direction generates two residual circulation cells (denoted by the two counter rotating cells) that cause a decay of the coastline perturbation. (c) Same as (b), but now the alongshore gradient of the alongshore vorticity flux is visualized. Small arrows represent perturbed alongshore vorticity flux $v'\Omega$ and $V\omega'$. The alongshore gradient of the alongshore vorticity flux generates residual circulation cells that cause a growth of the coastline perturbation.

in the negative y-direction compared to those obtained in the case that $f = 0$. Hence, the residual circulation cells in the case that $f \neq 0$ cause both growth and migration of the coastline perturbation.

2.6.2 Magnitude of growth rate for large wave numbers

An interesting result mentioned in the previous section is that for $\gamma = 0$ the growth rate of perturbations with large wave numbers ($kL \gg 1$) tends to a constant. In this section the physics underlying this behavior will be investigated. Starting point is Equation (2.27), which shows that for $\gamma = 0$ the growth rate is proportional to $\partial < v' > /\partial y|$ at the transition line. The latter term scales as $k[V'_{res}]$, where $[V'_{res}]$ is the magnitude of $< v' >$ at the transition line. From the observed behavior of the growth rate for $kL \gg 1$ it thus follows that

$$[V'_{res}] \sim (kL)^{-1} \qquad \text{for } kL \gg 1$$

To understand this result, we next estimate for the large wave number case the scale of the residual velocity component $< u' >$ and from there the scale of the residual vorticity. The latter will allow a quantification of the main terms in the residaul vorticity balance

(2.36).

The scale $[u'_{res}]$ of $< u' >$ follows from continuity equation (2.21c). Using the observed fact that the cross-shore and longshore length scale of the perturbations are of the same order the result is

$$[U'_{res}] \sim (kL)^{-1} \qquad \text{for } kL \gg 1$$

Since $\omega' = \partial v'/\partial x - \partial u'/\partial y$ the magnitude $[\omega'_{res}]$ of the residual vorticity obeys

$$[\omega'_{res}] \sim \text{constant} \qquad \text{for } kL \gg 1$$

These results are used to analyze the residual vorticity balance (2.36). It was already argued that terms (1) and (4) are the dominant terms in this equation. Using this fact and applying the continuity equation yields the order estimate

$$< \omega' > \sim < u' \frac{\partial \Omega}{\partial x} > - \frac{1}{H}\frac{dH}{dx} < \Omega u' > + \frac{\partial}{\partial y} < \omega' V >$$

When $kL \gg 1$ the magnitude of the first two terms on the right-hand side scale as kL because

$$[u'_{M2}] \sim kL \qquad \text{for } kL \gg 1$$

due to boundary condition (2.22) and because the cross-shore length scale of the variables H and Ω is the shelf width L rather than k^{-1}. Since $< \omega' >$ becomes constant in this parameter regime the last term on the right-hand side has to balance the first two terms. Consequently, the scale $[\omega'_{M2}]$ of the perturbed vorticity ω'_{M2} behaves as

$$[\omega'_{M2}] \sim \text{constant} \qquad \text{for } kL \gg 1$$

The final point is to understand the behavior of $[\omega'_{M2}]$ by considering the tidal vorticity balance. The latter is obtained by projecting the vorticity equation (2.35) onto the M_2 tidal components. This yields

$$\frac{\partial \omega'_{M2}}{\partial t} + < u' > \frac{\partial \Omega}{\partial x} - \frac{\Omega}{H}\frac{dH}{dx} < u' > + V\frac{< \omega' >}{\partial y} - \frac{r}{H^2}\frac{dH}{dx}v'_{M2} + \frac{r}{H}\omega'_{M2} = 0$$

Here, $f = 0$ has been assumed and the continuity equation has been applied.
The magnitude $[v'_{M2}]$ of v'_{M2} can be estimated from the continuity equation and using that boundary condition (2.22) implies that $u'_{M2} \sim \partial x'_{\mathrm{t}}/\partial y$. The result is

$$[v'_{M2}] \sim (kL) \qquad \text{for } kL \gg 1$$

Using all previous estimates of the magnitudes of the various variables in the case $kL \gg 1$ shows that the main balance in the tidal vorticity equation is between the fourth and fifth term. This conclusion is also found if Coriolis parameter f is nonzero. The final picture is thus that the tidal frictional torque (the fifth term) generates tidal vorticity by balancing with the fourth term, which represents the alongshore gradient in the transfer of perturbed residual vorticity by the undisturbed tidal current. This residual vorticity is associated with a residual current pattern with magnitude of the velocity components that were given above and which result in the saturation of the growth rate curve (i.e., $\Gamma \sim$ constant for $kL \gg 1$).

2.6.3   Sensitivity of model results to bathymetry

In Section 2.4.3 the sensitivity to the parameters L and H_0 was shown. A larger L resulted in a shift of λ_0 to larger values (Figure 2.9(a)). In addition, the growth rate and phase speed were smaller.

In the previous section it was shown that the value of λ_0 is determined by the wave number for which the magnitude of the alongshore gradient in the mean alongshore perturbed vorticity flux equals the magnitude of the cross-shore gradient in the mean cross-shore perturbed vorticity flux. Increasing the width of the inner shelf (L) results in a decrease of the magnitude of the cross-shore gradient of the mean cross-shore vorticity flux (both Ω and $\partial/\Omega/\partial x$ decrease). Therefore, already for smaller values of the wave number the growth rate becomes positive. Furthermore, a larger L results in smaller growth rates because the basic state vorticity and perturbed vorticity are smaller. This results in a smaller mean perturbed vorticity flux and its convergence is also smaller. Hence, the magnitude of the residual currents, the magnitude of $q'_{(curr)}$ and the growth rate are smaller for a fixed value of the wavelength. In addition, a larger L implies that planetary vortex stretching is smaller and therefore the phase speed of the perturbations of the coastline decrease for increasing values of L.

An increase of H_0 resulted in an increase of λ_0 (Figure 2.10(a)). When varying H_0, the friction parameter r and the pressure gradient due to the gradient in the sea surface elevation S_2 were not changed. When increasing H_0, U at the transition line increases as well, while the magnitudes of Ω and $\partial\Omega/\partial x$ decrease. Consequently, for a fixed wavelength the magnitude of the alongshore gradient in the mean alongshore vorticity flux increases with respect to the cross-shore gradient of the mean cross-shore vorticity flux when H_0 becomes larger. Therefore, already for smaller values of the wave number the growth rate becomes positive.

2.6.4   Sensitivity of model results to forcing conditions

The results of Section 2.4.2 show that an increase of the shore-parallel tidal currents results in an increase of λ_0 and an increase of the growth rates (Figure 2.7(a)). This is because an increase of the basic state tidal velocity results in a linear increase of the friction parameter r. Furthermore, an increase of r results in an increase of the basic state vorticity and its gradient. Consequently, considering a perturbation with a fixed wavelength, both the cross-shore gradient of the mean perturbed vorticity flux in the cross-shore direction and the alongshore gradient of the mean perturbed vorticity flux in the alongshore direction increase when U becomes larger. This results in the generation of residual circulation cells with large magnitude of the residual currents and therefore to an increase of $q'_{(curr)}$ and the growth rate. Furthermore, because the alongshore gradient of the mean alongshore vorticity flux increases stronger than the cross-shore gradient of the mean cross-shore vorticity flux with increasing magnitude of U, also the wavelength with zero growth rate λ_0 increases with increasing magnitude of U.

2.6.5   Fastest growing mode when wave flux is included

Including the influence of the volumetric sediment flux that is solely due to waves on the growth rate of the perturbations of the coastline has a considerable influence on the results. For certain parameter combinations a fastest growing mode is obtained (Figures 2.11 and 2.12). The reason why a fastest growing is obtained is straightforward. The alongshore gradient of the perturbed volumetric sediment flux $q'_{(\text{wave})}$ cause a decay of the perturbations of the position of the coastline and this decay is quadratic in the wave number (Equation (2.27)). The tidal currents cause growth of the perturbations with wavelengths smaller than λ_0. The growth rate tends to a constant for decreasing wavelengths (increasing values of kL). If the diffusion parameter due to the influence of waves (defined in Equation (2.28)) is too large, the perturbations decay for all wavelengths. When the diffusion parameter is zero no fastest growing mode is obtained. The influence of a very small diffusion parameter becomes noticeable for large wave numbers. For small wave numbers the growth rate of the perturbations is not affected by the waves and the growth rate increases for increasing wave numbers. For large wave numbers a positive value of the diffusion parameter causes the perturbations to decay and the growth rate decreases for increasing wave numbers. For moderate values of the wave number there exists a wave number for which the growth rate neither increase or decreases when the wave number is changed. This is the fastest growing mode. Increasing the wave influence causes an increase of the wavelength of the preferred mode. In a similar way it can be explained why for constant wave influence and increasing magnitude of the tidal currents the wavelength of the preferred mode decreases.

2.7   Discussion and conclusions

In this chapter a simplified model was developed to study and analyze the initial evolution of alongshore periodic perturbations on an otherwise alongshore uniform coastline. The aim was to study the dynamics behind the rhythmic occurrence of barrier islands and whether the dependence of the length scale could be understood in term of basic physical mechanisms. The new aspect of this study was the role of tides in the possible generation of these rhythmic coastline undulations. The model described in this study is meant as a natural extension of the one-line models of *Komar* (1998); *Falqués* (2003); *Falqués and Calvete* (2005), who only considered the influence of waves on the initial coastline development. The influence of waves on the growth rate of the alongshore rhythmic perturbation of the coastline was modeled as a diffusive process and the formulations of *Komar* (1998) are used. Since no nonlinear analysis has been carried out, no results are obtained that describe the finite-amplitude behavior of the coastline perturbations.

In the experiments described in Section 2.4.1-2.4.3 the evolution of the perturbations of the coastline under influence of tides only was studied. The results described in Section 2.4.1 show that for typical Dutch shelf conditions the growth rates are negative for long wavelengths, $\lambda > 8$ km. For smaller wavelengths the growth rate is positive, i.e., the perturbation of the position of the coastline is amplified. Typical time scales of the growth rate are in the order of 100 years. The Coriolis force induces a migration of the perturbations in the order of 10 meter per year. The perturbations are migrating to the

right, when viewing in the seaward direction. Although the model results change qualitatively when parameters describing the bathymetry of the inner shelf and the magnitude of the basic state tidal currents are changed, the result that the growth rate is negative for large wavelengths and positive for small wavelengths is robust when varying these parameters.

The physical mechanism resulting in growth or decay of coastline perturbations and their migration rates can be understood with vorticity dynamics. There is a competition between the cross-shore gradient of the mean cross-shore vorticity flux, which acts stabilizing, and alongshore gradient of the mean alongshore vorticity flux, which acts destabilizing. The width of the inner shelf determines the cross-shore length scale over which the cross-shore vorticity fluxes vary, while the wavelength of the perturbation determines the length scale over which the alongshore vorticity fluxes vary. If the length scale in the alongshore direction is smaller than the length scale in the cross-shore direction, the growth rate is positive. When the alongshore length scale is larger than the cross-shore length scale, a negative growth rate is obtained.

When the diffusion parameter due to the influence of sediment transported by waves is zero, the model does not predict a fastest growing mode because no damping mechanism is present for the small-scale perturbations. Including the influence of waves on the stability of the coastline results in the emergence of a fastest growing mode. The model results predict that under constant wave conditions the preferred length scale is smaller in regions where the alongshore tidal currents are stronger. This is observed along the Frisian Islands (Figure 2.13(b)). Furthermore, the model predicts that an increase of the diffusion parameter due to waves, while keeping the tidal current amplitude constant, results in a fastest growing mode with a larger wavelength. Along the Georgia Bight, when moving from the shelf of North Carolina to the shelf of Georgia, wave influence decreases and the tidal current amplitude increases (Figure 1.4). The model predicts that both effects result in a decrease of the preferred length scale. This is also observed.

For a realistic range of parameter values, a wavelength of the fastest growing mode in the range of 0 to 15 kilometer is obtained. This is in the range of observed length scales of barrier islands. However, the growth rates are small, in the order of hundred years. The predicted migration rates are up to ten meters per year. When wave influence is too strong, no growing perturbations are found. When the expression of *Komar* (1998) for the diffusion parameter due to waves is used (Equation (2.28)), the results show that for waves with H_b of 1 m the maximum angle of incidence of the waves is 40.42°. For smaller values the diffusion parameter is too large to have coastline perturbations that grow. However, *Falqués* (2003); *Falqués and Calvete* (2005) argue that the diffusion parameter in the model of *Komar* (1998) is a strong overestimation. Furthermore, the growth rate due to tides only ($\gamma = 0$) is also very small. As has been explained in Section 2.6.2, the alongshore gradient in the alongshore tidal vorticity flux counteracts the generation of tidal vorticity due to frictional torques. Therefore, for small wavelengths the generation of perturbed mean vorticity due to the perturbation of the position of the coastline is small and this results in the generation of only small residual currents. The predicted residual currents for a coastline perturbation of 500 meter and a wavelength of 3 km, are in the order of 10^{-3} ms^{-1}. The residual currents obtained with the present model seem to underestimate the magnitude of observed residual currents. Because the sediment flux

due to the influence of tides is linear in the mean alongshore velocity also the sediment flux due to tides is small and the evolution of the position of the coastline is small. Initial results suggest that adding horizontal turbulent mixing terms in the momentum equations increases the growth rate of coastline perturbations with at least a factor 10. In that case, the perturbations also grow when the diffusion parameter due to waves is much larger. Hence, a much smaller angle of incidence of the waves is possible. Still it is found that perturbations with small wavelengths grow and perturbations with long wavelengths decay.

Appendix

2.A   Parameters in the flow over topography problem

The parameters U_{ij} in Equation (2.31) read

$$U_{12} = 1 \tag{2.A-1a}$$

$$U_{11} = \frac{1}{H}\frac{dH}{dx} \tag{2.A-1b}$$

$$U_{10} = -k^2 + \frac{1}{H}\frac{d^2H}{dx^2} - \frac{1}{H^2}\left(\frac{dH}{dx}\right)^2 \tag{2.A-1c}$$

$$U_{02} = ikV + \frac{r}{H} \tag{2.A-1d}$$

$$U_{01} = \frac{ikV}{H}\frac{dH}{dx} \tag{2.A-1e}$$

$$
\begin{aligned}
U_{00} = &-ik^3V + \frac{ikV}{H}\frac{d^2H}{dH^2} - \frac{ikV}{H^2}\left(\frac{dH}{dx}\right)^2 \\
&+ \frac{ik\hat{f}}{H}\frac{dH}{dx} + \frac{ik}{H}\frac{\partial V}{\partial x}\frac{dH}{dx} - ik\frac{\partial^2 V}{\partial x^2} \\
&- \frac{k^2 r}{H} + \frac{r}{H^2}\frac{d^2H}{dx^2} - \frac{2r}{H^3}\left(\frac{dH}{dx}\right)^2
\end{aligned}
\tag{2.A-1f}
$$